EFFICIENT RECOMPUTATION OF MARGINAL LIKELIHOOD UPON ADDING TRAINING DATA IN GAUSSIAN PROCESSES AND SIMULATOR FUSION

Anonymous authors
Paper under double-blind review

ABSTRACT

To reduce generalization loss in line with the bias-variance trade-off, machine learning engineers should construct models based on their knowledge of the modeling target and, as training data increases, choose more flexible models with reduced dependence on that knowledge. To achieve this automatically, methods have been proposed to determine the amount of model's assumed prior knowledge directly from training data, rather than relying solely on an engineer's intuition. A widely studied approach involves using both a flexible model and a knowledge-dependent simulator, selectively incorporating simulator-generated data into the flexible model's training data. While neural networks have been used as flexible models, Gaussian Processes (GPs) are also candidates due to their flexibility and ability to output prediction uncertainty. However, direct methods for adding simulator-generated data to GPs training data remain unstudied. The SoD method, the closest alternative, often adds inappropriate data due to its assumption about the true distribution. On the other hand, the log marginal likelihood is a theoretically grounded metric when viewed as a model selection criterion for incorporating data generated from a simulator into the training data. However, calculating this metric for GPs is computationally expensive. To overcome this, we propose a faster method computing log marginal likelihood by considering the Cholesky factor and matrix element dependencies. Experiments indicate that metrics using log likelihood outperform SoD and other basic methods.

1 INTRODUCTION

One of the ultimate objectives of machine learning models is to reduce generalization loss. According to the bias-variance trade-off, the generalization loss, when employing Mean Squared Error (MSE) as the loss function, can be decomposed into terms of bias and variance. There is a trade-off between bias and variance, with very flexible models having low bias and high variance, and relatively rigid models having high bias and low variance. The model with the optimal predictive capability is the one that leads to the best balance between bias and variance (Bishop & Nasrabadi (2006)).

The strength of a model's rigidity or assumptions can either be determined manually by AI engineers or adjusted automatically from data. The latter is likely to achieve a more appropriate balance. There are two categories of methods to automatically adjust the strength of model assumptions from training data. The first category embeds assumptions directly into the model, adjusting their strength as hyperparameters. The second category involves preparing a separate model with strong assumptions and adjusting its influence on the main model. The specific methods of the former include L1 regularization, L2 regularization, and recent Physics-Informed Neural Networks(Raissi et al. (2019)). While this category of methods is applicable to parametric models, it is difficult to apply to non-parametric models like GPs mentioned later. The specific methods of the latter category include Auto Data Augmentation (Cubuk et al. (2019; 2020); Ho et al. (2019); Lim et al. (2019)) (for more details, see Appendix A.4) and selectively adding generated data from simulators to training data. Since this category controls the strength of assumptions not through the model's loss function but through training data, it can be applied whether the model is parametric or non-parametric. Within this category, although Auto Data Augmentation is efficient, the knowledge transferred from the

simulator must be expressed in the form of a policy. On the other hand, the method of selectively adding generated data has no restrictions on the format of the applicable simulator. Hence, we focus on the latter method of selectively adding generated simulator data to the training data.

When adjusting the strength of a model's assumptions, a flexible model with fewer assumptions is required as the prediction model before increasing the model's assumptions. In previous research, neural networks have been used as such models. While neural networks are powerful predictive models, their predictions are essentially point estimates, making it challenging to determine how much confidence to place in those predictions. Consequently, in recent years, GPs with deep structures replicating neural networks or CNNs have been proposed (Duvenaud (2014); Van der Wilk et al. (2017); Wilson et al. (2016)). GPs generate predictions along with confidence levels, offering a method that indicates how much trust can be placed in the predictions. By devising the kernel functions of the GPs, one can replicate deep learning models such as fully connected layers or CNNs. Research is advancing on models that retain the predictive power of neural networks while also providing a measure of prediction reliability. A drawback of GPs is their computational intensity, but as we will discuss later, this research alleviates that. In summary, if we can use GPs instead of neural networks as the predictive model before increasing model assumptions, we can develop a method that can automatically adjust the model's assumptions and also understand the reliability of the predictions.

However, a direct method of selectively adding simulator-generated data to training data when using GPs as the predictive model has not been studied. The closest approach is a technique called Subset of Data (SoD). SoD addresses the problem that GPs take a long time to compute because they use all the training data for each prediction by reducing the training data to only essential data. The criterion for selecting important data is the diversity of the training data. Various methods to measure this diversity have been proposed (Seeger et al. (2003); Lawrence et al. (2002); Lalchand & Faul (2018)). For more details, see Appendix A.1.

However, when using the diversity within training data as a criterion to selectively add simulator-generated data to the training data, data that deviates from the training data tends to be selected from the simulator-generated data. This may lead to preferentially adopting parts of the simulator's generation distribution that deviate from the true distribution, which in turn could potentially degrade the predictions of the GPs.

Bias-variance trade-off cannot be directly measured because we do not have knowledge of the true underlying distribution. Instead, we rely on indirect metrics. One such metric is the log marginal likelihood, which assesses the model's fit to the data and the balance of complexity as discussed in (Bishop & Nasrabadi (2006)). Optimizing the log marginal likelihood indirectly contributes to achieving a favorable balance between bias and variance. Therefore, we propose using the negative log marginal likelihood[1] of the GPs as a criterion when selectively adding simulator-generated data to the training data. The negative log marginal likelihood is a metric that measures the model's fit to the training data and has a theoretical foundation that it matches, on average, the Kullback–Leibler (KL) divergence between the true distribution and the model's distribution. For more details, see Appendix G, H and (Shlens (2007)). Furthermore, evaluating each candidate training data point using the negative log marginal likelihood can be time-consuming, so we propose a method for fast computation by considering the Cholesky update and the dependencies between matrix elements. Specifically, using our method, the computational cost to select generated data to add to the training set can be reduced from $O(M^3N + M^2N^2 + MN^3)$ to $O(M^2N + MN^2)$ where N is the number of true training data and M is the number of data generated by the simulator.

The contributions of this research are as follows:

1. We proposed using the negative log marginal likelihood of the GPs as a criterion when selectively adding simulator-generated data to the training data.

2. We proposed an algorithm to efficiently compute the negative log marginal likelihood when selecting training data.

[1]While the terms 'negative' and 'log' in 'negative log marginal likelihood' can be added as needed during optimization, for simplicity in this paper, it may also be referred to as 'marginal likelihood'. Additionally, the 'negative log marginal likelihood' is sometimes called 'type II likelihood' or 'free energy'.

2 METRICS

The aim of this study was to achieve an optimal balance between data and knowledge. The proposed approach employs GPs as a data-driven method and simulators as knowledge-driven models. To assess this optimal balance, we use the log marginal likelihood of the model as a metric, which approximates the KL divergence between the predictive distribution and the true distribution. (For an explanation of the approximation, refer to Appendix G) The method of achieving this balance involves sampling data from the simulator and adding it to the GPs' training data while checking the metric. We anticipate that if the simulator deviates significantly from the true distribution, or if there is already sufficient training data, adding that data to the GPs won't increase the log marginal likelihood. Consequently, such data would be rejected, resulting in a balanced distribution between the data and knowledge.

The process of the proposed method is straightforward. First, the hyperparameters of the GPs are learned using training data. Next, data $(\mathbf{x}, y)$ is sampled from the generative model[2] and added to the training data of the GPs. We measure the log marginal likelihood of the GPs, and if it improves, we accept the sampled data as valid training data, otherwise, we discard it. This process is repeated until no continuous improvement is observed or until all generated data has been examined. The GPs that possess both the original training data and the accepted generated data serve as our final prediction model.

In Section 2.1, we derive the marginal likelihood when adding the training data candidates generated from the simulator. In Section 3, we propose a method to quickly compute that marginal likelihood.

2.1 MARGINAL LIKELIHOOD OF GPS WHEN SYNTHETIC DATA IS ADDED

We define the symbols as follows: $\mathbf{x} \in \mathbb{R}^d$ is a random variable, $\mathbf{X}^N = (\mathbf{x}_1, \mathbf{x}_2, \ldots, \mathbf{x}_N)$ are N independent random variables following the same distribution, $y \in \mathbb{R}^1$ is a random variable, and $\mathbf{y}^N = (y_1, y_2, \ldots, y_N)$ are N independent random variables following the same distribution. Let $(\mathbf{X}^N, \mathbf{y}^N)$ be the training data and $(\mathbf{X}^{m^*}, \mathbf{y}^{m^*})$ be the m training data candidates generated from the simulator. Note that M is the total number of data generated from the simulator, and m is the number of training data candidates generated by the simulator up to the current step, as data is greedily added to the training set. We also denoted the star in $(\mathbf{X}^{m^*}, \mathbf{y}^{m^*})$ to explicitly indicate that it is not a sample from the true distribution.

As we mentioned at the beginning of Section 2, in order to evaluate samples from the generative model, we determine the marginal likelihood of the GP when such a sample is added. The negative log marginal likelihood (the free energy) of the discriminative model when pseudo data is added was $F_{m^*} = -\log p(\mathbf{y}^N | \mathbf{X}^N, \mathbf{y}^{m^*}, \mathbf{X}^{m^*})$. (Refer to Appendix H for the derivation.) In the case of GPs, since the predictive distribution can be analytically determined (see Appendix I), the marginal likelihood $p(\mathbf{y}^N | \mathbf{X}^N, \mathbf{y}^{m^*}, \mathbf{X}^{m^*})$ is also trivially obtained. To define the notation, let's express the joint distribution of synthetic data and training data as follows:

$$\begin{pmatrix} y_{1^*} \\ \vdots \\ y_{m^*} \\ y_1 \\ \vdots \\ y_N \end{pmatrix} \sim \mathcal{N}\left(\begin{pmatrix} 0 \\ \vdots \\ 0 \\ 0 \\ \vdots \\ 0 \end{pmatrix}, \begin{matrix} \mathbf{x}_{1^*} \\ \vdots \\ \mathbf{x}_{m^*} \\ \mathbf{x}_1 \\ \vdots \\ \mathbf{x}_N \end{matrix} \left(\begin{array}{c|c} \begin{matrix} \mathbf{x}_{1^*}{}^{3} \cdots \mathbf{x}_{m^*} \\ \mathbf{K}_{m^*} + \sigma^2 \mathbf{I}^{4} \end{matrix} & \begin{matrix} \mathbf{x}_1 \cdots \mathbf{x}_N \\ \mathbf{K}_{N,m^*} \end{matrix} \\ \hline \mathbf{K}_{N,m^*}^{\mathsf{T}} & \mathbf{K}_N + \sigma^2 \mathbf{I} \end{array} \right) \right). \tag{1}$$

Here, each $\mathbf{K}$ is the kernel of the corresponding rows and columns of $\mathbf{x}$. Using this notation, the free energy when synthetic data is added as training data is expressed as $p(\mathbf{y}^N | \mathbf{X}^N, \mathbf{y}^{m^*}, \mathbf{X}^{m^*}) = \mathcal{N}(\mathbf{K}_{N,m^*}^{\mathsf{T}} [\mathbf{K}_m + \sigma^2 \mathbf{I}]^{-1} \mathbf{y}^{m^*}, [\mathbf{K}_N + \sigma^2 \mathbf{I}] - \mathbf{K}_{N,m^*}^{\mathsf{T}} [\mathbf{K}_m + \sigma^2 \mathbf{I}]^{-1} \mathbf{K}_{N,m^*})$.

[2] In this paper, the terms 'simulator' and 'generative model' are used interchangeably.

[3] $\mathbf{x}_{1^*} \ldots \mathbf{x}_{m^*}, \mathbf{x}_1 \ldots \mathbf{x}_N$ represent the input variables for the kernel function that constructs the covariance matrix.

[4] Different-sized identity matrices appear in the paper, but the size is easily inferred from the context, so they are all uniformly denoted as $\mathbf{I}$.

Next, as a metric to determine whether to add the $m+1$-th data to where m pieces of synthetic data have been adopted, we will explain the free energy when the $m+1$-th synthetic data is added. Let's define the notation of the covariance matrix by adding $\mathbf{x}_{m+1^*}$ to Equation 1 as follows:

$$\begin{pmatrix} y_{1^*} \\ \vdots \\ y_{m^*} \\ y_{m+1^*} \\ y_1 \\ \vdots \\ y_N \end{pmatrix} \sim \mathcal{N}\left(\begin{pmatrix} 0 \\ \vdots \\ 0 \\ 0 \\ 0 \\ \vdots \\ 0 \end{pmatrix}, \begin{matrix} \mathbf{x}_{1^*} \\ \vdots \\ \mathbf{x}_{m^*} \\ \mathbf{x}_{m+1^*} \\ \mathbf{x}_1 \\ \vdots \\ \mathbf{x}_N \end{matrix} \left(\begin{array}{c|c} \begin{matrix} \mathbf{x}_{1^*} \cdots \mathbf{x}_{m^*} \; \mathbf{x}_{m+1^*} \\ \mathbf{K}_{m+1^*} + \sigma^2\mathbf{I} \end{matrix} & \begin{matrix} \mathbf{x}_1 \cdots \mathbf{x}_N \\ \mathbf{K}_{N,m+1^*} \end{matrix} \\ \hline \mathbf{K}_{N,m+1^*}^{\mathsf{T}} & \mathbf{K}_N + \sigma^2\mathbf{I} \end{array} \right) \right). \tag{2}$$

At this time, the free energy can be simply extended as: $F_{m+1^*} = -\log p(\mathbf{y}^N|\mathbf{X}^N, \mathbf{y}^{m^*}, \mathbf{X}^{m^*}) = -\log \mathcal{N}(\mathbf{K}_{N,m+1^*}^{\mathsf{T}}[\mathbf{K}_{m+1^*} + \sigma^2\mathbf{I}]^{-1}\mathbf{y}^{m+1}, [\mathbf{K}_N + \sigma^2\mathbf{I}] - \mathbf{K}_{N,m+1^*}^{\mathsf{T}}[\mathbf{K}_{m+1^*} + \sigma^2\mathbf{I}]^{-1}\mathbf{K}_{N,m+1^*})$.

For subsequent sections, let's expand the content of the free energy as follows:

$$F_{m+1^*} = \frac{1}{2}\left(\mathbf{y}^N\boldsymbol{\mu}_{m+1}\right)^{\mathsf{T}}\boldsymbol{\Sigma}_{m+1}^{-1}\left(\mathbf{y}^N - \boldsymbol{\mu}_{m+1}\right)\frac{1}{2}\log|\boldsymbol{\Sigma}_{m+1}| - \frac{N}{2}\log 2\pi, \tag{3}$$

$$\boldsymbol{\mu}_{m+1} = \mathbf{K}_{N,m+1^*}^{\mathsf{T}}[\mathbf{K}_{m+1^*} + \sigma^2\mathbf{I}]^{-1}\mathbf{y}^{m+1}, \tag{4}$$

$$\boldsymbol{\Sigma}_{m+1} = [\mathbf{K}_N + \sigma^2\mathbf{I}] - \mathbf{K}_{N,m+1^*}^{\mathsf{T}}[\mathbf{K}_{m+1^*} + \sigma^2\mathbf{I}]^{-1}\mathbf{K}_{N,m+1^*}. \tag{5}$$

The overall procedure of the algorithm is to randomly draw a generated data in sequence and formally add the $m+1$-th generated data to the training data if $F_{m+1^*} < F_{m^*}$, and discard it otherwise. Section 3 will explain an algorithm to perform this evaluation quickly.

3 An Algorithm for Reducing the Computational Cost of Free Energy Update

In order to rapidly compute equation 3, there are two challenges. The first one is to compute $\mathbf{K}_{m+1^*}^{-1} + \sigma^2\mathbf{I}$ in the mean (Equation 4). Though the computation of $\mathbf{K}_{m+1^*}^{-1} + \sigma^2\mathbf{I}$ can be efficiently determined through the Cholesky decomposition $\mathbf{K}_{m+1^*} + \sigma^2\mathbf{I} = \mathbf{L}_{m+1}\mathbf{L}_{m+1}^{\mathsf{T}}$ (where $\mathbf{L}_{m+1}$ is an $(m+1)\times(m+1)$ lower triangular matrix), the computational cost of obtaining $\mathbf{L}_{m+1^*}$ still remains $O(m^3)$. Hence, the total computational cost, even if pseudo-samples are adopted every time, amounts to $O(M^4)$ for incorporating M data points. This makes the computation challenging. However, by utilizing $\mathbf{L}_m$ from the previous step, the computation of $\mathbf{L}_{m+1}$ can be achieved in $O(m^2)$, and the total computational cost can be kept within $O(M^3)$. This technique is called Cholesky Update (Osborne (2010)). For other existing acceleration techniques, refer to Appendix A.3. The second one is that the inverse matrix of the free energy variance-covariance matrix, $\boldsymbol{\Sigma}_{m+1}^{-1}$, appearing in the first term on the right side of Equation 3, requires a matrix multiplication cost of $O(m^2N + mN^2)$ and $O(N^3)$ for the inversion even when the efficiently updated $\mathbf{L}_{m+1}$ is used (Osborne (2010)). Thus, the total amounts to $O(M^3N + M^2N^2 + MN^3)$, exceeding the allowable range. However, we propose a new algorithm which passes through the Cholesky decomposition of the variance-covariance matrix $\boldsymbol{\Sigma}_{m+1} = \mathbf{V}_{m+1}\mathbf{V}_{m+1}^{\mathsf{T}}$, and reuses $\mathbf{V}_m$ from the previous step for calculating $\mathbf{V}_{m+1}$[5]. The algorithm achieves a computational complexity of $O(mN + N^2)$ per step, with a total cost of $O(M^2N + MN^2)$, keeping it within the quadratic order for N. Once the Cholesky factor $\mathbf{V}_{m+1}$ is determined, the second term $|\boldsymbol{\Sigma}_{m+1}|$ in Equation 3 can also be immediately computed.

[5]Osborne (2010) proposed an efficient method to compute $\mathbf{L}_{m+1}$ from $\mathbf{L}_m$ in $O(m^2)$ for the Cholesky factor $\mathbf{K}_{m+1^*} + \sigma^2\mathbf{I} = \mathbf{L}_{m+1}\mathbf{L}_{m+1}^{\mathsf{T}}$. In contrast, we propose an efficient method to derive $\mathbf{V}_{m+1}$ from $\mathbf{V}_m$ in $O(mN + N^2)$ for $\boldsymbol{\Sigma}_{m+1} = \mathbf{V}_{m+1}\mathbf{V}_{m+1}^{\mathsf{T}}$.

3.1 COMPUTING $\mathbf{K}_{m+1^*}^{-1} + \sigma^2\mathbf{I}$

First, we explain how to efficiently compute the Cholesky factor $\mathbf{L}_{m+1}$ of $\mathbf{K}_{m+1^*}^{-1} + \sigma^2\mathbf{I}$ from $\mathbf{L}_m$. $\mathbf{K}_{m+1^*}$, as shown in Equation 6, possesses a structure extended by the kernel vector $\mathbf{k}_{m+1^*}$ and scalar k_{m+1^*} due to the added pseudo-data $\mathbf{x}_{m+1^*}$ to the covariance matrix $\mathbf{K}_{m^*}$ prior to the addition:

$$\mathbf{K}_{m+1^*} + \sigma^2\mathbf{I} = \begin{array}{c} \\ \mathbf{x}_{1^*} \\ \vdots \\ \mathbf{x}_{m^*} \\ \mathbf{x}_{m+1^*} \end{array} \begin{array}{c} \begin{array}{cc} \mathbf{x}_{1^*} \cdots \mathbf{x}_{m^*} & \mathbf{x}_{m+1^*} \end{array} \\ \left(\begin{array}{c|c} \mathbf{K}_{m^*} & \mathbf{k}_{m+1^*} \\ \hline \mathbf{k}_{m+1^*}^\mathsf{T} & k_{m+1^*} \end{array}\right) \end{array} + \sigma^2\mathbf{I}. \tag{6}$$

Here, we block partition the Cholesky factor $\mathbf{L}_{m+1}$ into three regions in the same manner:

$$\mathbf{L}_{m+1} = \begin{array}{c} \\ 1 \\ \vdots \\ m \\ m+1 \end{array} \begin{array}{c} \begin{array}{cc} 1 \cdots m & m+1 \end{array} \\ \left(\begin{array}{c|c} \mathbf{L}_{11} & \mathbf{0} \\ \hline \mathbf{l}_{21}^\mathsf{T} & l_{22} \end{array}\right) \end{array}. \tag{7}$$

Using the Cholesky factor update relations from Osborne (2010), $\mathbf{L}_{m+1}$ can be efficiently obtained using $\mathbf{L}_m$ as follows:

$$\begin{aligned} \mathbf{L}_{11} &= \mathbf{L}_m, & (8)\\ \mathbf{l}_{21} &= \mathbf{L}_m \backslash \mathbf{k}_{m+1^*}, & (9)\\ l_{22} &= \sqrt{k_{m+1^*} + \sigma^2 - \mathbf{l}_{21}^\mathsf{T}\mathbf{l}_{21}}. & (10) \end{aligned}$$

Here, $\mathbf{l}_{21} = \mathbf{L}_m \backslash \mathbf{k}_{m+1^*}$ is obtained by solving the equation $\mathbf{L}_m\mathbf{l}_{21} = \mathbf{k}_{m+1^*}$ for $\mathbf{l}_{21}$. This computation can be efficiently performed in $O(m^2)$ using back-substitutions (Seeger (2004)). The computational cost of the cholesky factor update (equations 8, 9, 10) is dominated by equation 9, and as a result, $\mathbf{L}_{m+1}$ can be computed from $\mathbf{L}_m$ in $O(m^2)$. Once $\mathbf{L}_{m+1}$ is determined, the mean term (equation 4) $(\mathbf{L}_{m+1}\mathbf{L}_{m+1}^\mathsf{T})^{-1}\mathbf{y}^{m+1^*}$ can also be computed in $O(m^2)$ by performing back-substitution twice.

3.2 COMPUTING INVERSE OF COVARIANCE MATRIX $\mathbf{\Sigma}_{m+1}^{-1}$

Once the Cholesky factor $\mathbf{\Sigma}_{m+1} = \mathbf{V}_{m+1}\mathbf{V}_{m+1}^\mathsf{T}$ is obtained, the first term in equation 3 can be computed by back-substitution in $O(N^2)$, and the second term, which is the product of the diagonal components of the Cholesky factor, can be computed in $O(N)$. Here, we describe a method to efficiently compute $\mathbf{V}_{m+1}$ using $\mathbf{V}_m$.

The covariance matrix can be transformed as follows:

$$\begin{aligned} \mathbf{V}_{m+1}\mathbf{V}_{m+1}^\mathsf{T} &= [\mathbf{K}_N + \sigma^2\mathbf{I}] - \mathbf{K}_{N,m+1^*}^\mathsf{T}[\mathbf{K}_{m+1^*} + \sigma^2\mathbf{I}]^{-1}\mathbf{K}_{N,m+1^*} & (11)\\ &= [\mathbf{K}_N + \sigma^2\mathbf{I}] - \mathbf{K}_{N,m+1^*}^\mathsf{T}\left(\mathbf{L}_{m+1}\mathbf{L}_{m+1}^\mathsf{T}\right)^{-1}\mathbf{K}_{N,m+1^*} & (12)\\ &= [\mathbf{K}_N + \sigma^2\mathbf{I}] - \left(\mathbf{L}_{m+1}^{-1}\mathbf{K}_{N,m+1^*}\right)^\mathsf{T}\left(\mathbf{L}_{m+1}^{-1}\mathbf{K}_{N,m+1^*}\right). & (13) \end{aligned}$$

Here, if we let $\mathbf{L}_{m+1}^{-1}\mathbf{K}_{N,m+1^*} = \mathbf{A}_{m+1}$, we want to show that it actually has the structure:

$$\mathbf{A}_{m+1} = \left(\begin{array}{c} \mathbf{A}_m \\ \hline \mathbf{a}_{m+1}^\mathsf{T} \end{array}\right). \tag{14}$$

Upon rearranging terms, it can be written as $\mathbf{L}_{m+1}\mathbf{A}_{m+1} = \mathbf{K}_{N,m+1^*}$. The explicit structures of $\mathbf{L}_{m+1}$ and $\mathbf{K}_{N,m+1^*}$ can be represented as follows:

$$\left(\begin{array}{c} \mathbf{L}_m \\ \hline \mathbf{l}_{m+1}^\mathsf{T} \end{array}\right)\mathbf{A}_{m+1} = \left(\begin{array}{c} \mathbf{K}_{N,m^*} \\ \hline \mathbf{k}_{N,m+1}^\mathsf{T} \end{array}\right). \tag{15}$$

When solving this for each column of $\mathbf{A}_{m+1}$ using the back-substitution method, it is observed that the components of each column are only influenced by the components above them in $\mathbf{L}_{m+1}$ and $\mathbf{K}_{N,m+1^*}$. Therefore, the influences of $\mathbf{l}_{m+1}^\mathsf{T}$ and $\mathbf{k}_{N,m+1}^\mathsf{T}$ are limited to the final row, resulting in the form described in Equation 14. Here, the nth component of $\mathbf{a}_{m+1}^\mathsf{T}$, $a_{m+1,n}$, is defined as follows. Let $\mathbf{l}_{m+1}^\mathsf{T} = (\mathbf{l}_{m+1,\leq m}^\mathsf{T} | l_{m+1,m+1})$, the vector excluding the last element $a_{m+1,n}$ of the nth column of $\mathbf{A}_{m+1}$ be $\mathbf{a}_{m,n}$, and the nth component of $\mathbf{k}_{N,m+1}^\mathsf{T}$ be $k_{m+1,n}$. Then,

$$a_{m+1,n} = \frac{1}{l_{m+1,m+1}}\left\{k_{m+1,n} - (\mathbf{l}_{m+1,\leq m}^\mathsf{T}\mathbf{a}_{m,n})\right\} \tag{16}$$

can be obtained.

The second term of Equation 13 is expressed as $\mathbf{A}_{m+1}^\mathsf{T}\mathbf{A}_{m+1}$, but by leveraging the structure of Equation 14, it can be separated into $\mathbf{A}_{m+1}^\mathsf{T}\mathbf{A}_{m+1} = \mathbf{A}_m^\mathsf{T}\mathbf{A}_m + \mathbf{a}_{m+1}\mathbf{a}_{m+1}^\mathsf{T}$. Substituting this in, we get

$$\mathbf{V}_{m+1}\mathbf{V}_{m+1}^\mathsf{T} = [\mathbf{K}_N + \sigma^2\mathbf{I}] - \left(\mathbf{A}_m^\mathsf{T}\mathbf{A}_m + \mathbf{a}_{m+1}\mathbf{a}_{m+1}^\mathsf{T}\right). \tag{17}$$

From Equation 13, it is known that $[\mathbf{K}_N + \sigma^2\mathbf{I}] - \left(\mathbf{A}_m^\mathsf{T}\mathbf{A}_m\right) = \mathbf{V}_m\mathbf{V}_m^\mathsf{T}$, hence

$$\mathbf{V}_{m+1}\mathbf{V}_{m+1}^\mathsf{T} = \mathbf{V}_m\mathbf{V}_m^\mathsf{T} - \mathbf{a}_{m+1}\mathbf{a}_{m+1}^\mathsf{T} \tag{18}$$

holds true. With this form, the rank-one downdate (Seeger (2004)) can be utilized to update from $\mathbf{V}_m$ to $\mathbf{V}_{m+1}$ with a computational complexity of $O(N^2)$. The derived algorithm is summarized in Algorithm 1 in Appendix B.

4 Experiments

4.1 Comparison with Other Methods

Firstly, in order to measure the accuracy of the proposed method in regression, we compare the mean squared error (MSE) with existing methods. The first dataset utilizes one-dimensional artificial data. We aim to replicate a scenario where we can obtain training data from the true distribution and data from a partially correct custom simulator. For specific examples of situations where this occurs, refer to Appendix C. In this experiment, the distributions of the true and the simulator are given by the following equations:

$$\begin{aligned} True &: 4\cos(1.5x)\exp(-0.1x) + 4\arctan(x-10) + \mathcal{N}(0, 0.5), \\ Sim. &: 4\cos(1.5x) + 4\arctan(x-10) + \mathcal{N}(0, 0.5). \end{aligned}$$

It is assumed that during the simulator's construction, the existence of the decay term $\exp(-0.1x)$ was not recognized. The proposed algorithm aims to selectively incorporate only the matching data from simulator data into the training data. In our experiments, we utilize three types of data: training data, simulation data, and test data. To ensure these data sets do not overlap, they were constructed as follows: From the true distribution, 2000 data points were generated, and randomly $50, 100, 200, \ldots, 900$ points were chosen as training data. From the remaining data, 1000 data points were randomly selected as test data. As simulator data, 10000 data points were generated from the simulation distribution. In most of our experiments, we repeated the experiment 10 times, reporting the average and standard deviation. The training and test data were reselected randomly from the 2000 data points generated from the true distribution in each trial.

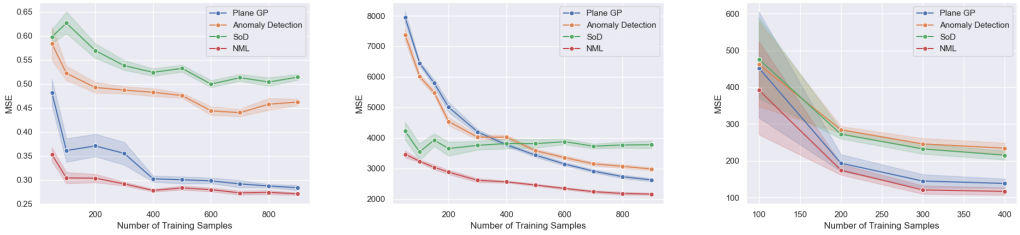

(a) 1d data (b) 8d data (c) Concrete compressive strength

Figure 1: Comparison of the proposed method (NML) with other methods

The second dataset is eight-dimensional synthetic data. The distributions for the true and the simulator are as follows:

$$
\begin{aligned}
True \quad &: \quad 4\cos 1.5x_1 + 3\sin 0.5x_2 + 4x_3 + (x_4 - 5)^2 + 3\cos 3x_5 + 3\sin x_6 + x_7^2 - (x_8 - 15)^2 \\
&\quad +150\exp\left(-(x_1 - 10)^2\right) + \mathcal{N}(0, 1.0), \\
Sim. \quad &: \quad 4\cos 1.5x_1 + 3\sin 0.5x_2 + 4x_3 + (x_4 - 5)^2 + 3\cos 3x_5 + 3\sin x_6 + x_7^2 - (x_8 - 15)^2 \\
&\quad +\mathcal{N}(0, 1.0).
\end{aligned}
$$

The methods for generating training data, simulation data, and test data are the same as for the one-dimensional data mentioned above. However, to reduce learning time in the eight-dimensional data, we generated and used 1000 data points as simulation data. For details on the kernel and training parameters, refer to Appendix D.

The third dataset used is real-world data. We evaluated our method using the concrete compressive strength dataset, a standard dataset in regression tasks (Yeh (2007)). The concrete compressive strength dataset aims to predict the target variable, concrete compressive strength, using eight explanatory variables related to materials. As for data generated from a simulator, out of 500 datasets, the target variable was modified to be $+20$ from its original value for $3/4$ of the data, while the remaining $1/4$ were kept as the original data. This simulates a scenario where a simulator tends to overestimate the concrete compressive strength due to some factors. The number of training data points was set at $100, 200, 300, 400$, and the test data comprised 100 data points. For details on the kernel and training parameters, refer to Appendix E.

As comparative methods, in addition to the standard GPs, we implemented a method using anomaly detection as a naive benchmark and SoD (Lalchand & Faul (2018)). Lalchand & Faul (2018) described in Appendix A.1, promote diversity of training data. The termination condition was set to accept until half of all simulator data were accepted. The method using anomaly detection is a naive approach that excludes outliers in the simulator using a GP trained on true training data. The criterion for determining if it's an outlier is calculated by feeding all input data $\mathbf{X}$ from the simulator to the GP to predict its distribution and then using the likelihood of all the output data $\mathbf{y}$ from the simulator. If the likelihood is below a certain threshold, it is considered an outlier and is not added to the training data. The threshold was selected from $(0.2, 0.4, 0.6, 0.8, 1.0)$ through cross-validation. This method can be seen as not sequentially adding simulator data to training data in the proposed method, and also measures the significance of sequential addition.

Figure 1 shows the results of comparing the accuracy of regression predictions on three datasets. The horizontal axis of each graph represents the number of real training data used for learning, while the vertical axis represents MSE on test data, with a lower value being better. The solid lines represent the average of 10 trials for each method, and the shaded regions represent the standard deviation. For both datasets, improvements were observed with the proposed method, negative marginal likelihood (NML), compared to the Plane GP. As can be seen in Section 4.2, this is because only beneficial data from the simulator-generated data were added to the training data. On the other hand, SoD showed a reduction in MSE compared to Plane GP. As discussed in Section 4.2, this is likely because SoD prioritized diversity, leading to the inclusion of simulator-generated data that is distant from the training data and deviates from the true distribution.

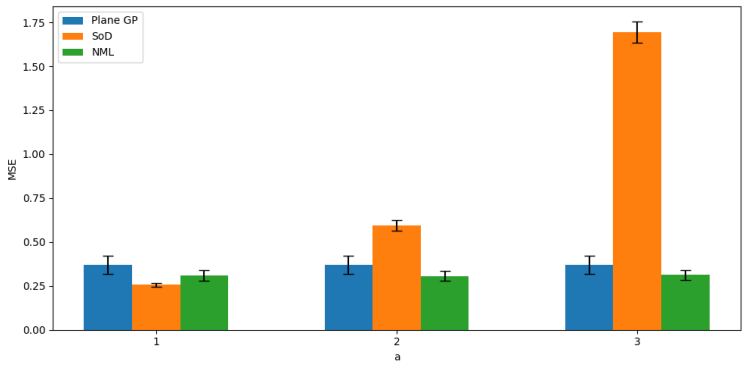

Figure 2: Impact of the difference between the training data candidate distribution and the true distribution on the MSE of each method.

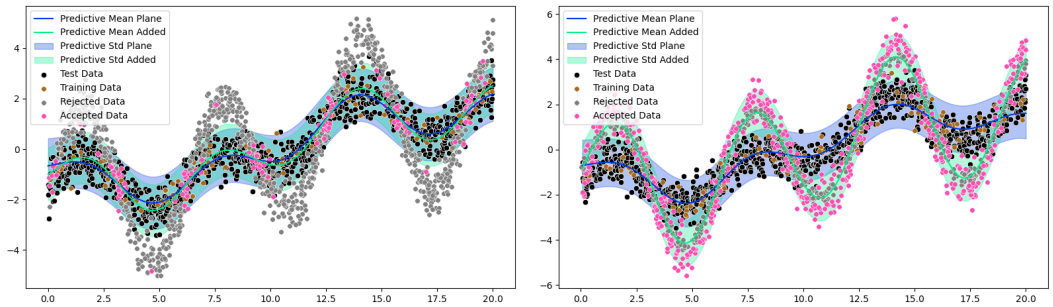

(a) NML (b) SoD

Figure 3: Data adopted for training from the training data candidates. The x-axis represents x and the y-axis represents y. Predictive Mean Plane and Predictive Std Plane are the average and standard deviation of Plane GP predictions. Predictive Mean Added and Predictive Std Added are the average and standard deviation of predictions for NML or SoD. Accepted Data are those adopted from the training data candidates, and the gray points were not adopted.

4.2 Limitation of Marginal Likelihood

We aim to clarify the effective range of marginal likelihood and SoD. Specifically, unlike our proposed method which doesn't require training data to be from the true distribution, SoD assumes it is. We seek to understand the effects on both methods when training data diverges from the true distribution.

To this end, we altered the distance between the simulator distribution and the true distribution, observing the prediction accuracy of each method. Specifically, the true and simulator distributions were set as follows:

$$\begin{aligned} \text{True} &: \sin(x) + \arctan(x-10) + \mathcal{N}(0, 0.5) \\ \text{Sim.} &: a \times \sin(x) + \arctan(x-10) + \mathcal{N}(0, 0.5) \end{aligned}$$

Here, a is an experimental parameter to adjust the distance between the simulator and true distributions. In this experiment, $a = [1, 2, 3]$. When $a = 1$, the training data candidates are assumed to be sampled from the true distribution, and as a increases, the distribution of training data candidates diverges from the true distribution. The number of true training data was set to 50, the number of training data candidates generated from the simulator was 1000, and the number of test data was 1,000. We resampled all this data 10 times and showed the average and standard deviation of MSE on a graph. For details on the kernel and training parameters, refer to Appendix E.

The results are shown in Figure 2. First, when $a = 1$ and the distributions of training data candidates and the true distribution match, both NML and SoD had a lower MSE than Plane GP. Among

them, SoD had a lower MSE than NML. This suggests that the diversity of training data in the SoD approach is important under this condition. However, as a increases to 2 and 3, and the training data candidate distribution deviates from the true distribution, the MSE of SoD increases, while the MSE of NML remains smaller than Plane GP. For $a = 3$, data included in the training data from the training data candidates and data that was rejected are visualized in Figure 3.

As SoD aims to enhance the diversity of training data, it accepts training data candidates that deviate from the true distribution that training and test data follow, resulting in a deterioration in MSE due to the predictions being influenced by these data. On the other hand, NML mainly accepts training data candidates close to the true distribution, leveraging the correct part of the simulator distribution, $arctan(x - 10)$. Accepting only the beneficial parts and stopping there implies that we have achieved our original goal, which was to automatically adjust the strength of the model's assumptions, that is, to find an appropriate balance between the strong assumptions of the simulator and the lax assumptions of the GPs. From these results, when training data deviates from the true distribution and aligns with simulator-generated data, using marginal likelihood to fit training data can yield samples close to the true distribution, benefiting prediction tasks. In contrast, the SoD metric, focusing on training data diversity, can include data far from the true distribution in simulator-generated data, negatively impacting predictions.

4.3 Computation Time

We experimentally verify the computational complexity reduction effect of the proposed method. We compare the method that goes through the Cholesky decomposition of the covariance matrix proposed in Section 3 $\mathbf{\Sigma}_{m+1} = \mathbf{V}_{m+1}\mathbf{V}_{m+1}^{\mathrm{T}}$ with the method that does not. The CPU was an Intel CORE i7 vPro 8th Gen, and 32GB memory was used. The results are shown in Figure 4. The horizontal axis represents the number of training data N, and the vertical axis represents the time taken for learning in hours. With the proposed computational technique, the increase in computational time is gradual even as the number of training data increases, while without it, there is a sharp increase. This result confirms that the computational time order of the conventional method is $O(N^3)$, whereas the computational time order of the proposed method is $O(N^2)$. Furthermore, the gentle increase in computational time of the proposed method suggests that the coefficient of $O(N^2)$ is small.

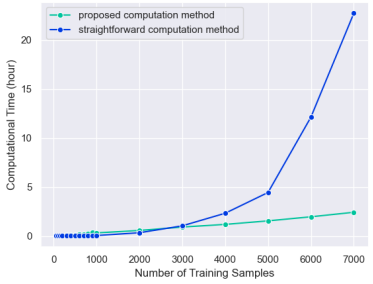

Figure 4: Computational Time

5 Conclusion

We propose using the negative log marginal likelihood of the GPs as a criterion when selectively adding simulator-generated data to the training data in order to adjust the extent to which prior knowledge is incorporated into GPs. Through experiments, it was confirmed that the proposed method extracts only the correct knowledge from the simulator and improves the MSE. By only accepting the beneficial components and halting, we have effectively balanced the strong assumptions of the simulator with the lenient assumptions of the GPs, achieving our original objective. Moreover, by taking into account the Cholesky factor and the dependency of matrix elements, We proposed an algorithm that reduces the computational cost of selecting training data candidates from $O(M^3N+M^2N^2+MN^3)$ to $O(M^2N+MN^2)$. As a limitation, the algorithm we proposed is specialized for regression models with Gaussian likelihood, and its extension to classification models and other likelihood models is not straightforward. We are planing to address this in the future.

References

Hirotogu Akaike. Information theory and an extension of the maximum likelihood principle. In *Selected papers of hirotugu akaike*. Springer, 1998.

Christopher M Bishop and Nasser M Nasrabadi. *Pattern recognition and machine learning*. Springer, 2006.

TD Bui, CV Nguyen, and RE Turner. Streaming sparse gaussian process approximations. In *Neural Information Processing Systems (NeurIPS)*, 2017.

Ching-An Cheng and Byron Boots. Incremental variational sparse gaussian process regression. In *Neural Information Processing Systems (NeurIPS)*, 2016.

Lehel Csató and Manfred Opper. Sparse on-line gaussian processes. *Neural computation*, 2002.

Ekin D Cubuk, Barret Zoph, Dandelion Mane, Vijay Vasudevan, and Quoc V Le. Autoaugment: learning augmentation strategies from data. In *Computer Vision and Pattern Recognition (CVPR)*, 2019.

Ekin D Cubuk, Barret Zoph, Jonathon Shlens, and Quoc V Le. Randaugment: Practical automated data augmentation with a reduced search space. In *Computer Vision and Pattern Recognition Workshops*, 2020.

David Duvenaud. *Automatic model construction with Gaussian processes*. PhD thesis, University of Cambridge, 2014.

James Hensman, Nicolo Fusi, and Neil D Lawrence. Gaussian processes for big data. In *Uncertainty in Artificial Intelligence (UAI)*, 2013.

Daniel Ho, Eric Liang, Xi Chen, Ion Stoica, and Pieter Abbeel. Population based augmentation: efficient learning of augmentation policy schedules. In *International Conference on Machine Learning (ICML)*, 2019.

Diederik P Kingma and Jimmy Ba. Adam: a method for stochastic optimization. In *International Conference on Learning Representations (ICLR)*, 2015.

Vidhi Lalchand and AC Faul. A fast and greedy subset-of-data (sod) scheme for sparsification in gaussian processes. *International Workshop on Bayesian Inference and Maximum Entropy Methods in Science and Engineering*, 2018.

Neil Lawrence, Matthias Seeger, and Ralf Herbrich. Fast sparse gaussian process methods: the informative vector machine. In *Neural Information Processing Systems (NeurIPS)*, 2002.

Sungbin Lim, Ildoo Kim, Taesup Kim, Chiheon Kim, and Sungwoong Kim. Fast autoaugment. In *Neural Information Processing Systems (NeurIPS)*, 2019.

Duy Nguyen-Tuong, Jan Peters, and Matthias Seeger. Local gaussian process regression for real time online model learning and control. In *Neural Information Processing Systems (NeurIPS)*, 2008.

Michael A Osborne. *Bayesian Gaussian processes for sequential prediction, optimisation and quadrature*. PhD thesis, Oxford University, UK, 2010.

Barnabás Póczos and Jeff Schneider. Nonparametric estimation of conditional information and divergences. In *Artificial Intelligence and Statistics*, 2012.

Maziar Raissi, Paris Perdikaris, and George E Karniadakis. Physics-informed neural networks: A deep learning framework for solving forward and inverse problems involving nonlinear partial differential equations. *Journal of Computational physics*, 2019.

Matthias Seeger. Low rank updates for the cholesky decomposition. Technical report, 2004.

Matthias W Seeger, Christopher KI Williams, and Neil D Lawrence. Fast forward selection to speed up sparse gaussian process regression. In *International Workshop on Artificial Intelligence and Statistics (AISTATS)*, 2003.

Jonathon Shlens. Notes on kullback-leibler divergence and likelihood theory. *Systems Neurobiology Laboratory*, 92037:1–4, 2007.

Edward Snelson and Zoubin Ghahramani. Sparse gaussian processes using pseudo-inputs. In *Neural Information Processing Systems (NeurIPS)*, 2005.

Michalis Titsias. Variational learning of inducing variables in sparse gaussian processes. In *Artificial intelligence and statistics*, 2009.

Mark Van der Wilk, Carl Edward Rasmussen, and James Hensman. Convolutional gaussian processes. In *International Workshop on Artificial Intelligence and Statistics (AISTATS)*, 2017.

Andrew Gordon Wilson, Zhiting Hu, Ruslan Salakhutdinov, and Eric P Xing. Deep kernel learning. In *Artificial intelligence and statistics*, 2016.

I-Cheng Yeh. Concrete Compressive Strength. UCI Machine Learning Repository, 2007.

A Related Works

A.1 Subset of Data

Subset of Data (SoD) is a method that selects important data from candidate training data for GPs. By generating training data candidates from simulators built using domain knowledge, the extent of domain knowledge reflection into GPs can be adjusted by determining which data and how much of it is included in the training data. SoD evaluates the training data candidates based on a metric and greedily adds the highest-ranked ones. The metric for selecting important data is the diversity of the training data (Seeger et al. (2003); Lawrence et al. (2002); Lalchand & Faul (2018)). Various methods to measure this diversity have been proposed. Lawrence et al. (2002) uses the difference in entropy between predictive distributions with and without a specific training data point as its metric. Seeger et al. (2003) uses the KL divergence between predictive distributions with and without a specific training data point. Lalchand & Faul (2018) employs its unique diversity metric. Specifically, when predicting with a GPs using the already accepted training data, they add data candidates to the training set where the sum of the squared error and the prediction uncertainty is large. As the training data candidates move farther from the already adopted training data, both the prediction squared error and uncertainty increase. Thus, candidates that enhance the diversity of the training data are chosen. These methods assume that training data candidates are sampled from the true distribution and can ensure diversity within the training set. However, in the context of adjusting the amount of domain knowledge introduced, training data candidates are sampled from simulators using domain knowledge, which means there could be regions that deviate from the true distribution. Consequently, data deviating from the true distribution might be prioritized, causing predictive distributions to diverge. Lawrence et al. (2002) employs a method using GPs classification, while Seeger et al. (2003) uses a sparse GPs method. Given this, we choose Lalchand & Faul (2018), which can be directly applied to standard GPs regression, to represent the SoD method and compare it with our proposed method in experiments.

A.2 Sparse Gaussian Processes

similarly to the Subset of Data, there are methods to generate a small number of pseudo-training data for reducing the training data. Some of these methods, like the proposed approach, use the log marginal likelihood as a metric to generate pseudo-training data (Titsias (2009); Snelson & Ghahramani (2005)). However, none of these compute the exact log marginal likelihood. For example, (Titsias (2009)) developed sparse GPs to reduce training data by substituting the Gaussian process model from $p(\mathbf{f}|\mathbf{X})$ to $p(\mathbf{f}|\mathbf{f}^m)$, avoiding direct dependency of function values $\mathbf{f}$ on the training data $\mathbf{X}$, rather relying of function value $\mathbf{f}^m$ on the pseudo data. This change in the model altered the formula for marginal likelihood, which could not be computed quickly, leading to the use of a lower bound of marginal likelihood as the metric instead (Titsias (2009)). On the other hand, in our intended applications, all training data are available, so there is no need to alter the marginal likelihood. Our proposed acceleration method allows us to use the exact log likelihood as the metric. Similarly, (Snelson & Ghahramani (2005)) also uses an approximation of the marginal log likelihood, not the exact value, as the metric (Titsias (2009)).

A.3 RECOMPUTATION TECHNIQUES FOR GPS WHEN DATA IS ADDED

SoD evaluates the goodness of added training data candidates by sequentially adding them to the GP's training data and measuring the predictive distribution of the model using a metric. The computational effort needed to compute the predictive distribution when data is added has been researched in the domain of Online GPs. After training with N data points (after computing the inverse matrix with N data), an additional data point can be learned with an added computational effort of $O(N^2)$ using a technique called rank-one update (Nguyen-Tuong et al. (2008); Seeger (2004)). This technique is used in part in our method. However, even with this technique, it's not efficient to compute the inverse of the covariance matrix for the log marginal likelihood. In this study, we propose a method to efficiently compute it.

Since it takes $O(N^3)$ computational effort to compute the predictive distribution of a GPs, methods have been proposed that combine approximation techniques and online learning to reduce this. Among the approximation methods that use the inducing variable method and variational inference, methods to go online by mini-batch (Hensman et al. (2013); Cheng & Boots (2016)) and methods to go online by sequential Bayesian updates (Csató & Opper (2002); Bui et al. (2017)) have been proposed. Also, an online method that used a local GPs has been proposed (Nguyen-Tuong et al. (2008)). Although our study does not use these approximation methods to compute the log marginal likelihood without approximation, they may be utilized in the future to reduce computational effort.

A.4 AUTO-DATAAUGMENTATION

When Data Augmentation rules are considered as one of the inductive biases, one can interpret it as injecting domain knowledge, such as the rules of augmentation (like an image retains its class even when flipped), into the machine learning model. Notably, auto data augmentation (Cubuk et al. (2019; 2020); Ho et al. (2019); Lim et al. (2019)) explores optimal magnitudes and application probabilities of multiple data augmentations, like image flips and rotations, based on training data. This concept is similar to our proposed method. The difference lies in the fact that while auto data augmentation employs neural network classifiers as the discriminative model, our approach uses a GPs regression model. Moreover, auto data augmentation evaluates policies, while our method evaluates individual single data. Although potentially less efficient, our method offers versatility in situations where defining a policy is challenging. Our approach does not optimize the order of samples for evaluation. This is because, compared to the vast neural networks used in auto data augmentation, the GPs evaluations can be conducted in a shorter computation time. However, considering sample order optimization could be a consideration for future work if it becomes crucial.

B DETAILS OF THE PROPOSED ALGORITHM

The pseudo-code of the proposed algorithm is shown in Algorithm 1.

The hyperparameters of the input kernel function are pre-optimized using the true training data $(\mathbf{X}^N, \mathbf{y}^N)$ and remain fixed until the completion of Algorithm 1. While it is possible to relearn the kernel's hyperparameters using the selected generated data $(\mathbf{X}^{M^*}, \mathbf{y}^{M^*})$ and the original training data $(\mathbf{X}^N, \mathbf{y}^N)$ after applying Algorithm 1, this second round of learning has not been conducted in the experiments presented in this paper.

C USE CASES OF PARTIALLY CORRECT SIMULATORS

For instance, in semiconductor inspection algorithms, lasers are irradiated onto wafers to predict the presence or absence of foreign substances based on scattered light. Obtaining substantial real-world data is challenging due to the high experimental costs involved. While it is possible to simulate scattered light, accounting for the thermal effects caused by the laser heating the foreign substances is challenging. Therefore, there is a need to combine the limited real-world data with imperfect simulation data that does not consider thermal effects, to make accurate predictions. To generalize such a situation, we construct distributions for both the true distribution and a simulator that slightly deviates from it.

Algorithm 1 Selection of Samples Reducing Free Energy

Input: Training data $(\mathbf{X}^N, \mathbf{y}^N)$, simulator $p_S(y, \mathbf{x})$, GP kernel function
Output: Selected generated data $\left(\mathbf{X}^{M^*}, \mathbf{y}^{M^*}\right)$

compute $\mathbf{K}_N$
$\mathbf{V}_0 = Cholesky\left(\mathbf{K}_N + \sigma^2\mathbf{I}\right)$
while True **do**
  sample $(y_{m+1^*}, \mathbf{x}_{m+1^*}) \sim p_S(y, \mathbf{x})$
  if $m = 0$ **then**
    $\mathbf{L}_1 = \sqrt{k_{1^*} + \sigma^2}$
  else $\{m \geq 1\}$
    compute $\mathbf{k}_{m+1^*}$, k_{m+1^*}
    $\mathbf{L}_{m+1} = CholeskyFactorUpdate\left(\mathbf{L}_m, \mathbf{k}_{m+1^*}, k_{m+1^*} + \sigma^2\right)$
  end if
  compute $\mathbf{K}_{N,m+1^*}$
  Mean $\boldsymbol{\mu}_{m+1} = \mathbf{K}_{N,m+1^*}^{\mathsf{T}} \left(\mathbf{L}_{m+1}\mathbf{L}_{m+1}^{\mathsf{T}}\right)^{-1} \mathbf{y}^{m+1}$
  if $m = 0$ **then**
    $\mathbf{a}_1^{\mathsf{T}} = \mathbf{K}_{N,1^*}/\mathbf{L}_1$
    $\mathbf{A}_1 = \mathbf{a}_1^{\mathsf{T}}$
  else $\{m \geq 1\}$
    $\mathbf{a}_{m+1} = LastCholeskySolution\left(\mathbf{L}_{m+1}, \mathbf{A}_m, \mathbf{K}_{N,m+1^*}\right)$
    $\mathbf{A}_{m+1} = stack\left(\mathbf{A}_m, \mathbf{a}_{m+1}\right)$
  end if
  $\mathbf{V}_{m+1} = RankOneDowndate\left(\mathbf{V}_m, \mathbf{a}_{m+1}\right)$
  $\left(\mathbf{y}^N - \boldsymbol{\mu}_{m+1}\right)^{\mathsf{T}} \boldsymbol{\Sigma}_{m+1}^{-1} \left(\mathbf{y}^N - \boldsymbol{\mu}_{m+1}\right) = \left(\mathbf{y}^N - \boldsymbol{\mu}_{m+1}\right)^{\mathsf{T}} \left(\mathbf{V}_{m+1}\mathbf{V}_{m+1}^{\mathsf{T}}\right)^{-1} \left(\mathbf{y}^N - \boldsymbol{\mu}_{m+1}\right)$
  $|\boldsymbol{\Sigma}_{m+1}|$ = product of diagonal elements of $\mathbf{V}_{m+1}$
  $F_{m+1} = -\frac{1}{2}\left(\mathbf{y}^N - \boldsymbol{\mu}_{m+1}\right)^{\mathsf{T}} \boldsymbol{\Sigma}_{m+1}^{-1} \left(\mathbf{y}^N - \boldsymbol{\mu}_{m+1}\right) - \frac{1}{2}\log|\boldsymbol{\Sigma}_{m+1}| - \frac{N}{2}\log 2\pi$
  if $F_{m+1} < F_m$ **then**
    $\mathbf{X}^{m+1} = \mathbf{X}^{m^*} + \mathbf{x}_{m+1^*}$
    $\mathbf{y}^{m+1} = \mathbf{y}^{m^*} + y_{m+1^*}$
    $m++$
  else $\{F_{m+1} \geq F_m\}$
    reject $(y_{m+1^*}, \mathbf{x}_{m+1^*})$
    break if rejected R times consecutively
  end if
end while

D Details of kernels and training parameters in section 4.1

We employed the RBF kernel as the kernel for GPs regression. The initial values of the kernel parameters were set to $amplitude = 10$ and $length_scale = 10$. The variance of observation noise was 1.

The estimation of the above three parameters was carried out by maximum likelihood estimation using the true training data. For training parameters, we used Adam(Kingma & Ba (2015)) with a learning rate of 0.001, $\beta_1 = 0.9$, $\beta_2 = 0.999$, and $\epsilon = 1e-7$. The batch size was set to 1, and the number of iterations was 15,000. We did not optimize these training hyperparameters.

E Details of kernels and training parameters in section 4.2 and real data

We employed the RBF kernel as the kernel for GPs regression. The initial values of the kernel parameters were set to $amplitude = 1$ and $length\_scale = 1$. The variance of observation noise was 1. Estimation of these parameters was conducted using maximum likelihood estimation with true training data. For training parameters, we used Adam(Kingma & Ba (2015)) with a learning

rate of 0.01, $\beta_1 = 0.9$, $\beta_2 = 0.999$, and $\epsilon = 1e-7$. The batch size was set to 1, and the number of iterations was 2,000. These training hyperparameters were not optimized.

F ABLATION STUDY

Our proposed method used the free energy as a metric, and efficiently computed the computationally expensive inverse of the covariance matrix $\mathbf{\Sigma}_{m+1}^{-1}$ and its determinant $\|\mathbf{\Sigma}_{m+1}\|$ in the free energy equation 3. To verify whether it's truly necessary to compute the inverse and determinant of the covariance matrix, we conducted an ablation study.

We compared with two ablated methods. The first method removed the inverse of the covariance matrix from equation 3, resulting in $-\frac{1}{2}(\mathbf{y}^N - \boldsymbol{\mu}_{m+1})^\mathsf{T}(\mathbf{y}^N - \boldsymbol{\mu}_{m+1}) - \frac{1}{2}\log|\mathbf{\Sigma}_{m+1}| - \frac{N}{2}\log 2\pi$. The second method also eliminated the determinant term, yielding $-\frac{1}{2}(\mathbf{y}^N - \boldsymbol{\mu}_{m+1})^\mathsf{T}(\mathbf{y}^N - \boldsymbol{\mu}_{m+1}) - \frac{N}{2}\log 2\pi$. This approach is simply the squared error between the GPs (GP) prediction mean and the actual data. The constant term $\frac{N}{2}\log 2\pi$ does not influence data selection.

We varied the amount of training data, conducted a 10-cross validation, and compared the MSE of test data. The results are shown in Figure 5. The method without the inverse of the covariance matrix is labeled as w/o inverse, the one without the determinant is labeled as squared error, and our proposed method is labeled as NML. The results showed that MSE, which evaluates the full free

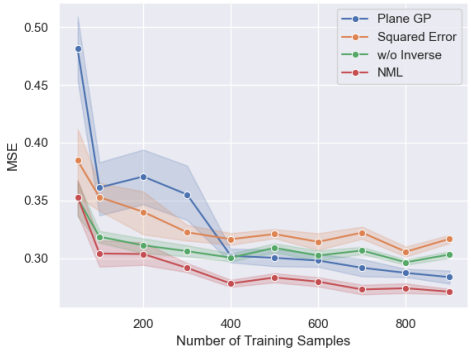

Figure 5: Comparison of MSE with ablated methods

energy, demonstrated more stable improvements than both the simple squared error and w/o inverse. From this, we can deduce that both the inverse of the covariance matrix $\mathbf{\Sigma}_{m+1}^{-1}$ and its determinant $\|\mathbf{\Sigma}_{m+1}\|$ significantly contribute to the improvement of MSE.

G NEGATIVE LOG MARGINAL LIKELIHOOD

In Bayesian statistics, free energy (negative log marginal likelihood) or generalization loss is used as a model evaluation metric. The free energy measures the model's fit to the training data, and model selection often involves either the free energy or its approximation, the BIC (Bayes Information criterion). The generalization loss measures the accuracy of the model's predictive distribution, and for model selection, cross-validation loss or the AIC (Akaike Information Criterion) (Akaike (1998)) are commonly used. In this study, we use the free energy as the metric for SoD.

We define the symbols as follows: $\mathbf{X} \in \mathbb{R}^d$ is a random variable, $\mathbf{X}^N = (\mathbf{X}_1, \mathbf{X}_2, \ldots, \mathbf{X}_N)$ are N independent random variables following the same distribution, $\mathbf{y} \in \mathbb{R}^1$ is a random variable, and $\mathbf{y}^N = (\mathbf{y}_1, \mathbf{y}_2, \ldots, \mathbf{y}_N)$ are N independent random variables following the same distribution. The free energy of the discriminative model (including GPs) is given by the following equation:

$$F = -\log p(\mathbf{y}^N | \mathbf{X}^N). \tag{19}$$

When the realized values of N training data are obtained in a regression task, the realized value of the model's free energy is $-\log p(\mathbf{y}^N = \mathbf{y}^N|\mathbf{X}^N = \mathbf{x}^N)$. Random variables are denoted in uppercase, and realized values are denoted in lowercase.

This metric is explained by the difference between the true distribution of the dataset and the inferred model distribution. If we denote the true distribution of the dataset as $q(\mathbf{y}^N|\mathbf{X}^N)q(\mathbf{X}^N)$ and the distribution in the discriminative model of the dataset as $p(\mathbf{y}^N|\mathbf{X}^N)$, the conditional KL-divergence (Póczos & Schneider (2012)) between the two distributions is

$$\begin{aligned} KL(q(\mathbf{y}^N|\mathbf{X}^N)||p(\mathbf{y}^N|\mathbf{X}^N)) &= \int q(\mathbf{X}^N) \int q(\mathbf{y}^N|\mathbf{X}^N) \log \frac{q(\mathbf{y}^N|\mathbf{X}^N)}{p(\mathbf{y}^N|\mathbf{X}^N)} d\mathbf{y}^N d\mathbf{X}^N \\ &= \mathbb{E}[F] + C. \end{aligned} \tag{20}$$

Where $\mathbb{E}[\cdot]$ denotes the average over samples from the true distribution and $C = \int q(\mathbf{y}^N|\mathbf{X}^N)q(\mathbf{X}^N) \log q(\mathbf{y}^N|\mathbf{X}^N) d\mathbf{X}^N d\mathbf{y}^N$ is a constant that does not depend on the model's distribution. Therefore, a smaller free energy F indicates that the inferred distribution approximates the true distribution well on average.

H Free Energy when Synthetic Data is Added in General

As mentioned at the beginning of Section 2, we want to measure whether the performance of the discriminative model improved by adding samples from the simulator to the training data of the discriminative model. We adopt free energy as a performance metric and extend the free energy of Equation 19 when samples are added from the generative model. If m samples from the generative model are represented by $(\mathbf{X}^{m^*}, \mathbf{y}^{m^*})$, then the predictive distribution given $(\mathbf{X}^{m^*}, \mathbf{y}^{m^*})$ in the model becomes $p(\mathbf{y}^N|\mathbf{X}^N, \mathbf{X}^{m^*}, \mathbf{y}^{m^*})$. The conditional KL-divergence (Póczos & Schneider (2012)) between $p(\mathbf{y}^N|\mathbf{X}^N, \mathbf{X}^{m^*}, \mathbf{y}^{m^*})$ and the true distribution can be transformed as follows:

$$\begin{aligned} KL(q(\mathbf{y}^N|\mathbf{X}^N) \quad || \quad & p(\mathbf{y}^N|\mathbf{X}^N, \mathbf{X}^{m^*}, \mathbf{y}^{m^*})) \\ &= \int q(\mathbf{X}^N) \int q(\mathbf{y}^N|\mathbf{X}^N) \log \frac{q(\mathbf{y}^N|\mathbf{X}^N)}{p(\mathbf{y}^N|\mathbf{X}^N, \mathbf{X}^{m^*}, \mathbf{y}^{m^*})} d\mathbf{y}^N d\mathbf{X}^N \\ &= \mathbb{E}[-\log p(\mathbf{y}^N|\mathbf{X}^N, \mathbf{X}^{m^*}, \mathbf{y}^{m^*})] + C. \end{aligned} \tag{21}$$

Therefore, if we define

$$F_{m^*} = -\log p(\mathbf{y}^N|\mathbf{X}^N, \mathbf{X}^{m^*}, \mathbf{y}^{m^*}) \tag{22}$$

then minimizing F_{m^*} will minimize $KL(q(\mathbf{y}^N|\mathbf{X}^N)||p(\mathbf{y}^N|\mathbf{X}^N, \mathbf{X}^{m^*}, \mathbf{y}^{m^*}))$ on average. Thus, we obtained F_{m^*} as a performance metric for the discriminative model when $(\mathbf{X}^{m^*}, \mathbf{y}^{m^*})$ is given. F_{m^*} is, then, the free energy when synthetic data is added.

I Basics of GPs Regression

Given an input $\mathbf{x}$, we define the feature vector of $\mathbf{x}$ as $\boldsymbol{\phi}(\mathbf{x}) = (\phi_0(\mathbf{x}), \phi_1(\mathbf{x}), \ldots, \phi_H(\mathbf{x}))^\mathsf{T}$. Considering the linear regression model $y = \mathbf{w}^\mathsf{T}\boldsymbol{\phi}(\mathbf{x})$ with weights $\mathbf{w} = (w_0, w_1, \ldots, w_H)$, for N input-output pairs, it can be described simultaneously using the design matrix $\boldsymbol{\Phi} = \left(\boldsymbol{\phi}(\mathbf{x}_1)^\mathsf{T}, \ldots, \boldsymbol{\phi}(\mathbf{x}_N)^\mathsf{T}\right)$, which can be written as $\mathbf{y} = \boldsymbol{\Phi}\mathbf{w}$. Here, $\mathbf{y} = (y_1, \ldots, y_N)^\mathsf{T}$.

Assume the weights $\mathbf{w}$ are drawn from a Gaussian distribution $\mathcal{N}(\mathbf{0}, \lambda^2\mathbf{I})$ with mean $\mathbf{0}$ and variance $\lambda\mathbf{I}$. Then, since $\mathbf{y}$ is a linear transformation of the Gaussian distributed vector $\mathbf{w}$ by the constant matrix $\boldsymbol{\Phi}$, $\mathbf{y} = \boldsymbol{\Phi}\mathbf{w}$ also follows a Gaussian distribution. The mean is given by $\mathbb{E}[\mathbf{y}] = \mathbb{E}[\boldsymbol{\Phi}\mathbf{w}] = \boldsymbol{\Phi}\mathbb{E}[\mathbf{w}] = \mathbf{0}$, and the covariance matrix is $\mathbb{E}[\mathbf{y}\mathbf{y}^\mathsf{T}] - \mathbb{E}[\mathbf{y}]\mathbb{E}[\mathbf{y}]^\mathsf{T} = \mathbb{E}[(\boldsymbol{\Phi}\mathbf{w})(\boldsymbol{\Phi}\mathbf{w})^\mathsf{T}] = \boldsymbol{\Phi}\mathbb{E}[\mathbf{w}\mathbf{w}^\mathsf{T}]\boldsymbol{\Phi}^\mathsf{T} = \lambda^2\boldsymbol{\Phi}\boldsymbol{\Phi}^\mathsf{T}$. As a result, the distribution of $\mathbf{y}$ becomes a multivariate Gaussian distribution, $\mathbf{y} \sim \mathcal{N}(\mathbf{0}, \lambda^2\boldsymbol{\Phi}\boldsymbol{\Phi}^\mathsf{T})$. By defining the covariance matrix as $\mathbf{K} = \lambda^2\boldsymbol{\Phi}\boldsymbol{\Phi}^\mathsf{T}$, the (n, n')

elements become $k(\mathbf{x}_n, \mathbf{x}_{n'}) = \phi(\mathbf{x}_n)^\mathsf{T}\phi(\mathbf{x}_{n'})$. Now, by constructing the kernel matrix $\mathbf{K}$ by directly defining the kernel function $k(\mathbf{x}_n, \mathbf{x}_{n'})$, there's no need to explicitly define the feature vector $\phi(\mathbf{x})$ (kernel trick). Here, the definition of the GPs is that for any set of N inputs $(\mathbf{x}_1, \ldots, \mathbf{x}_N)$, if the joint distribution $p(\mathbf{y})$ of the corresponding outputs $\mathbf{y} = (y_1, \ldots, y_N)$ follows a multivariate Gaussian distribution, the relationship between $\mathbf{x}$ and y is governed by a GPs. Now, $\mathbf{y} \sim \mathcal{N}(\mathbf{0}, \mathbf{K})$ is a GPs with mean $\mathbf{0}$ and covariance matrix $\mathbf{K}$. It should be noted that we can centered the mean of the observed data $\mathbf{y}$ at $\mathbf{0}$ without loosing generalization. For the training data $\mathbf{X}^N = (\mathbf{x}_1, \ldots, \mathbf{x}_N)$ and $\mathbf{y}^\mathbf{N} = (y_1, \ldots, y_N)^\mathsf{T}$, and the data we wish to predict $\bar{\mathbf{X}}^S = (\bar{\mathbf{x}}_1, \ldots, \bar{\mathbf{x}}_S)$, the joint distribution of the corresponding output $\bar{\mathbf{y}}^S = (\bar{y}_1, \ldots, \bar{y}_S)^\mathsf{T}$ is given by:

$$\begin{pmatrix} y_1 \\ \vdots \\ y_N \\ \bar{y}_1 \\ \vdots \\ \bar{y}_S \end{pmatrix} \sim \mathcal{N}\left(\begin{pmatrix} 0 \\ \vdots \\ 0 \\ 0 \\ \vdots \\ 0 \end{pmatrix}, \begin{matrix} \mathbf{x}_1 \\ \vdots \\ \mathbf{x}_N \\ \bar{\mathbf{x}}_1 \\ \vdots \\ \bar{\mathbf{x}}_S \end{matrix} \left(\begin{array}{c|c} \begin{matrix} \mathbf{x}_1 \cdots \mathbf{x}_N \\ \mathbf{K}_N + \sigma^2\mathbf{I} \end{matrix} & \begin{matrix} \bar{\mathbf{x}}_1 \cdots \bar{\mathbf{x}}_S \\ \bar{\mathbf{K}}_{S,N} \end{matrix} \\ \hline \bar{\mathbf{K}}_{S,N}^\mathsf{T} & \bar{\mathbf{K}}_S \end{array} \right) \right). \tag{23}$$

$\sigma^2\mathbf{I}$ represents the variance of observational noise, modeling the presence of noise in the training data. The predictive distribution can be analytically derived as

$$p(\bar{\mathbf{y}}^S | \bar{\mathbf{X}}^S, \mathbf{y}^N, \mathbf{X}^N) = \mathcal{N}(\bar{\mathbf{K}}_{S,N}^\mathsf{T}[\mathbf{K}_N + \sigma^2\mathbf{I}]^{-1}\mathbf{y}^N, \bar{\mathbf{K}}_S - \bar{\mathbf{K}}_{S,N}^\mathsf{T}[\mathbf{K}_N + \sigma^2\mathbf{I}]^{-1}\bar{\mathbf{K}}_{S,N}). \tag{24}$$